Electronic Supplementary Material (ESI) for Journal of Materials Chemistry C.

SUPPORTING INFORMATION

Short lead(II) soaps: from weakly fluorescent crystals to strongly phosphorescent and structurally varied vitreous phases. Thermal, structural and spectroscopic study.

Francisco J. Martínez-Casado,[a#] Miguel Ramos-Riesco,[b] José A. Rodríguez-Cheda,[b] Fabio Cucinotta,[c] Alejandro Fernández-Martínez,[d,e] Leoncio Garrido,[f] Emilio Matesanz,[g] and Leonardo Marchese.[c]

[a] MAX IV Laboratory, Lund University, SE-221 00 Lund, Sweden
[b] Departamento de Química Física I, Facultad de Ciencias Químicas, Universidad Complutense, 28040 Madrid, Spain
[c] Dipartimento di Scienze e Innovazione Tecnologica and Nano-SISTEMI Interdisciplinary Centre, Universitá del Piemonte Orientale "A. Avogadro", via Teresa Michel 11, I-15121 Alessandria, Italy
[d] CNRS, ISTerre, F-38041 Grenoble, France
[e] Univ. Grenoble Alpes, ISTerre, F-38041 Grenoble, France
[f] Departamento de Química Física, Instituto de Ciencia y Tecnología de Polímeros, Consejo Superior de Investigaciones Científicas (ICTP-CSIC), 28006 Madrid, Spain
[g] Centro de Asistencia a la Investigación – Difracción de Rayos X, Facultad de Ciencias Químicas, Universidad Complutense, 28040 Madrid, Spain

■ INDEX

- **Experimental** **2**
- **Results**
    1. **Differential Scanning Calorimetry (DSC)** **4**
    2. **X-ray Diffraction (XRD)** **6**
    3. **PDF analysis** **11**
    4. **Photoluminescence (PL)** **16**
    5. **C-13 CP/MAS Nuclear Magnetic Resonance (NMR)18**
    6. **Optical Microscopy** **19**
- **References** **20**

■ EXPERIMENTAL

Sample preparation. The methods of synthesis for the different salts are described in detail elsewhere,[1-3]and are valid for all of the compounds of the lead(II) alkanoates series.

Crystals suitable for single crystal X-ray studies of $Pb(C3)_2$, $Pb(C5)_2$, and $Pb(C6)_2$ were grown up by slow evaporation from ethanol solutions (for $Pb(C3)_2$ and $Pb(C5)_2$) and benzene (for $Pb(C6)_2$). The sizes of the single crystals are given in Table S2.

Differential Scanning Calorimetry (DSC). A TA Instruments DSC Model Q10 was used in this work. Tightly sealed aluminum volatile pans (in N_2 atmosphere) were used to scan at different heating rates (in dry nitrogen atmosphere at a gas flow of about 50 $mL \cdot min^{-1}$). An MT5 Mettler microbalance was used to weigh 10 mg of each sample (error: ± 0.001 mg). The calorimeter temperature was calibrated using In and Sn standard samples supplied by TA (purity > 99.999 % and > 99.9 %, respectively), and benzoic acid (purity > 99.97 %), supplied by the former NBS (lot 39i). Enthalpy was calibrated using the In and Sn standards.

The thermal data are shon in Table S1. DSC thermograms for $Pb(C5)_2$ are given in ref 4.

Single Crystal X-ray Diffraction (SCXRD). Synchrotron radiation SCXRD experiments were performed with a wavelength $\lambda = 0.9779$, for $Pb(C3)_2$ and $Pb(C5)_2$, and $\lambda = 0.7379$ Å, for $Pb(C6)_2$, at the BM16 Spanish beamline of European Synchrotron Radiation Facility (ESRF, in Grenoble, France) using a CCD detector (ADSCq210r), making phi scans while collecting the data. The oscillation range (Δ φ) used for each image was one degree. $Pb(C3)_2$ was measured at RT, and the other compounds at 100 K.

The structures were solved by direct methods and subsequent Fourier syntheses using the SHELXS-97 program, and were refined by the full-matrix least-squares technique against F^2, using the SHELXL-97 program.[5] Anisotropic thermal parameters were used to refine all non-H atoms. The H atoms were placed in idealized positions, in every case, and their parameters were not refined. An absorption correction was done for all of the compounds, due to the presence of lead.

The crystals suffered severe radiation damage in all of the cases and, together with the great difficulty to obtain good crystals (due to a weak bonding between lipidic layers), makes that the data statistics obtained by SCXRD are not as good as desirable for small molecules. However, the data are reliable and, as a proof of it, High Resolution Powder Diffraction was performed to confirm the structures by the Rietveld method (see pages 6-9).

The experimental parameters, crystal sizes, and main crystallographic data for the compounds studied are shown in Table S2.

Powder X-ray Diffraction (PXRD). High resolution powder diffraction (HRPD) measurements were performed for $Pb(C3)_2$, $Pb(C5)_2$, and $Pb(C6)_2$, in order to confirm the structures found by SCXRD. Besides, in the cases of $Pb(C5)_2$ and $Pb(C6)_2$ (measured at 100K by SCXRD), the structures were solved and refined at room temperature by the Rietveld method.

$Pb(C6)_2$ was analyzed at SpLine beamline (BM25A) of the Spanish CRG at the ESRF, with a fixed wavelength of (0.8266 ± 0.0001) Å, at room temperature. The powdered sample was placed inside a 0.5-mm-diameter glass capillary, which was rotated during exposure. Data collection was done in a 2θ-step scan mode with 0.015° step and 5 sec. acquisition time per point.

$Pb(C3)_2$ and $Pb(C5)_2$ were measured at room temperature in transmission mode in a Panalytical X'Pert PRO diffractometer equipped with a "hybrid monochromator" (a combination of a parabolic mirror and a Ge220 channel cut monochromator) and a fast RTMS detector X'Celerator (Cu $K\alpha 1$ radiation, 1.54056 Å, 45 kV, 40 mA). The measurement range of 2θ was from 2.5° to 85°, and step size 0.008°. The samples were prepared in 0.3 mm-diameter glass capillaries, and rotated during exposure. The measurements were carried out by accumulation of 10 diffractograms for these two compounds.

The main experimental parameters and crystallographic data for the compounds studied by PXRD are shown in Table S3.

XRD measurements as a function of temperature were carried out in reflection mode with a Panalytical X'Pert PRO MPD X-ray diffractometer with vertical goniometer θ/θ and RTMS X'Celerator detector equipped with a high-temperature camera Anton Paar HTK1200 (Cu Kα1 radiation, 1.54056 Å, 45 kV, 40 mA, Ni filter). In-situ XRPD scans were measured under still air conditions from 2θ = 2º-70º at several temperatures in the range from 25ºC to 95ºC during heating and cooling, after programming every temperature change at a rate of 3ºC/min.

High-energy X-ray Total Scattering and PDF Analysis. Finely powdered dry samples of the lead(II) salts were loaded into 1.0 mm diameter kapton capillaries. High-energy X-ray total scattering data acquisition was performed at beamline ID15B, at the ESRF. Scattering data were collected with a Mar133 CCD-detector using the Rapid-Acquisition Pair Distribution Function technique.[6] Samples, an empty capillary and the background were measured at RT from 0–25.0 $Å^{-1}$. The X-ray wavelength was refined using a CeO_2 standard (λ = 0.1419 Å). Corrections for sample-detector distance, tilt angle of the detector with respect to the direction of the incident radiation and polarization were performed using Fit2D.[7] Total scattering structure factors and Pair Distribution Functions (PDFs) were obtained using the PDFGetX3 software.[8]

UV-Vis Spectroscopy. UV-visible diffuse reflectance spectra were recorded using a Perkin-Elmer Model Lambda 900 spectrophotometer, equipped with a diffuse reflectance sphere accessory (DR-UV-vis). Prior to the analysis, the solid compounds were dispersed in an anhydrous BaSO4 matrix (10% in weight).

Steady-state emission spectra were recorded on a Horiba Jobin Yvon Model IBH FL-322 Fluorolog 3 spectrometer equipped with a 450-W xenon arc lamp, double-grating excitation and emission monochromators (2.1 nm/mm dispersion; 1200 grooves/mm) and a Hamamatsu Model R928 photomultiplier tube. Emission and excitation spectra were corrected for source intensity (lamp and grating) and emission spectral response (detector and grating) by standard correction curves. Time-resolved measurements up to ~ 5 μs were performed using the time-correlated single-photon counting (TCSPC) option on the Fluorolog 3 spectrometer. A NanoLED (370 nm; full width at half maximum (fwhm) = 1.2 ns) with repetition rates between 10 kHz and 1 MHz was used to excite the sample. The excitation source was mounted directly on the sample chamber at 90° to a double-grating emission monochromator (2.1 nm/mm dispersion; 1200 grooves/mm) and signals were collected using an IBH Data Station Hub photon counting module. Data analysis was performed using the commercially available DAS6 software (Horiba Jobin Yvon IBH). For excited state lifetimes > 5 μs, a SpectraLED was used as excitation source (460 nm; fwhm = 1.2 ns) and data collection and analysis was made as described above.

The samples, in the crystal and glass phases, were measured at 77 K and at RT.

C-13 CP/MAS NMR. Solid state C-13 NMR measurements were performed in a Bruker Avance^{TM} 400 spectrometer (Bruker Analytik GmbH Karlsrube, Germany) equipped with a 89 mm wide bore, 9.4 T superconducting magnet (C-13 Larmor frequency at 100.61MHz). Powdered samples were placed in 4 mm zirconia rotors (about 60 mg of sample). All reported data were acquired at two temperatures, first at (296 ± 0.1) K and then after thermal equilibrium was reached at (343 ± 0.1) K. Once at this temperature, the sample was quenched in CO_2 ice/i-propanol and placed in the magnet, having the probe at T: 298.6-296.5 K, and measured again at 296 K. We used a standard Bruker double resonance 4 mm cross-polarization (CP)/magic angle spinning (MAS) NMR probe head using a 90º C-13 pulse length of 4.2 □s. The C-13 spectra were acquired with 1 ms CP contact time, 5 s recycle delay, MAS spinning rates of 6.5 kHz and 1000 transients. High-power proton decoupling of 75 kHz was used. The NMR spectra were evaluated with the spectrometer manufacture's software package XWIN-NMR^{TM}. All free-induction decays were subjected to standard Fourier transformation with 5 Hz line broadening and phasing. The chemical shifts were externally referenced to adamantane (29.5 ppm) secondary to TMS (0.0 ppm).

Polarized Light Microscopy. A Carl Zeiss-Jena polarizing optical microscope model pol-30-G0527 was used, equipped with a LINKAM hot stage, model THMS600, connected to a LINKAM programmable temperature-controller, model TMS94.

■ RESULTS

1) Differencial Scanning Calorimetry (DSC)

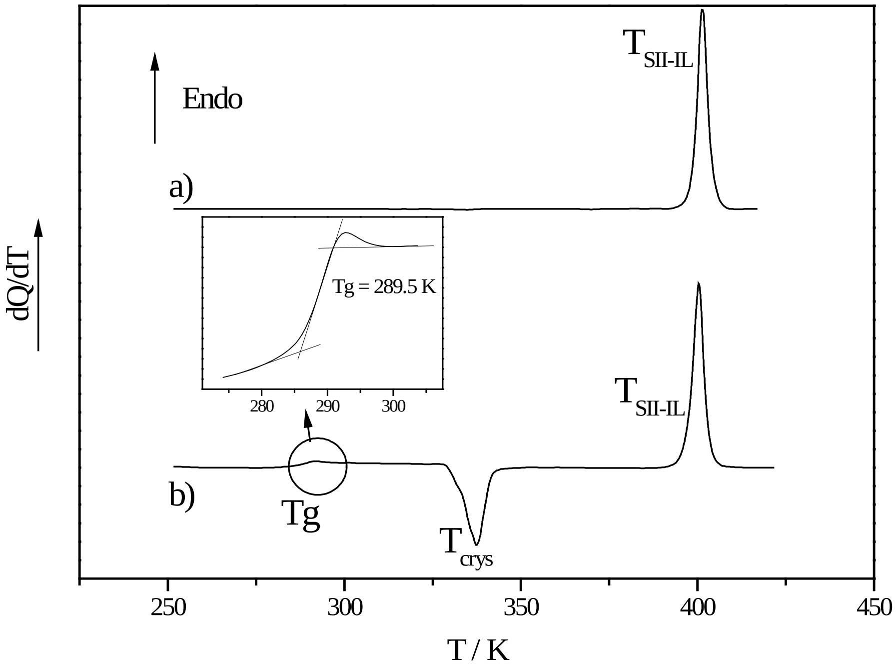

Figure S1. Thermograms of $Pb(C3)_2$ in the first (a) and second and next heatings (b), both registered at 5 K·min^{-1}. The transition temperature of SII-IL, and Tg and T_{crys} are indicated in the plot.

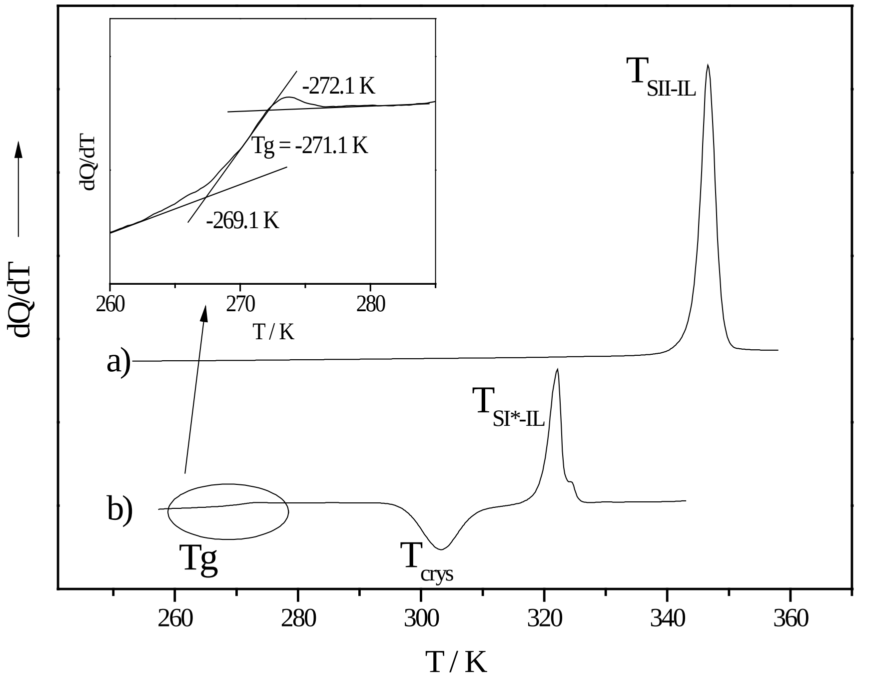

Figure S2. Thermograms of $Pb(C4)_2$ in the first (a), and second heating (b), registered at 1.25 K·min^{-1}. The transition temperatures of SII-IL SI*-IL, and Tg and T_{crys} are indicated in the plot. It is worth noting that in The second heating a metastable phase (SI*) is obtained, which melts at a lower temperature and with a smaller enthalpy than in the case of SII. The process is reversible and the thermal behavior of the first heating is recovered after 2 months at RT.

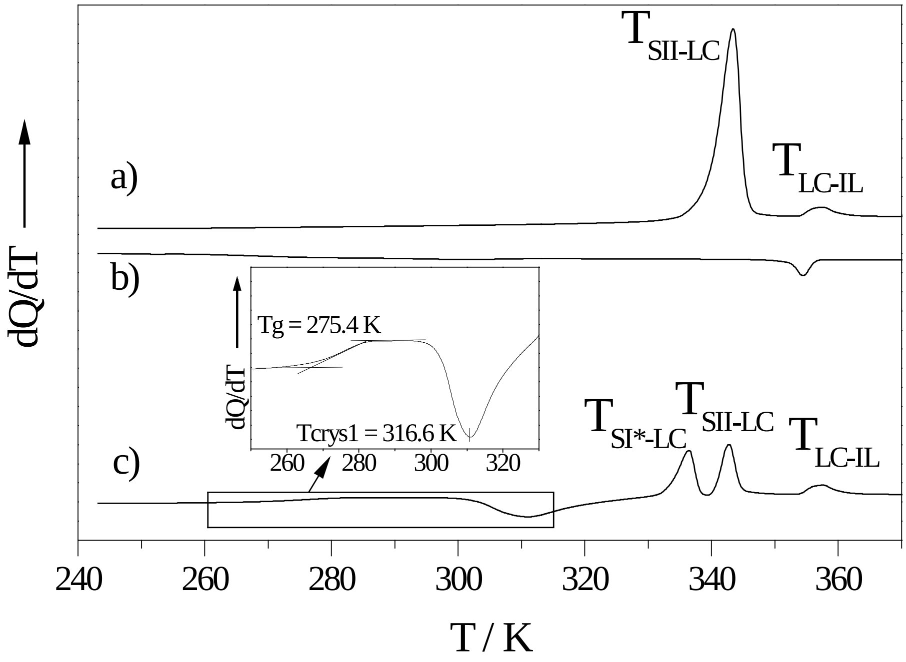

Figure S3. Thermograms of Pb(C6)$_2$ in the first heating (a), cooling (b) and second heating (c), all of them registered at 5 K·min^{-1}The transition temperatures of SI*-LC, SII-LC and LC-IL, and Tg, T_{crys1} and T_{crys2} are indicated in the plot. SI* corresponds to a metastable phase that appears, depending on the heating rate.

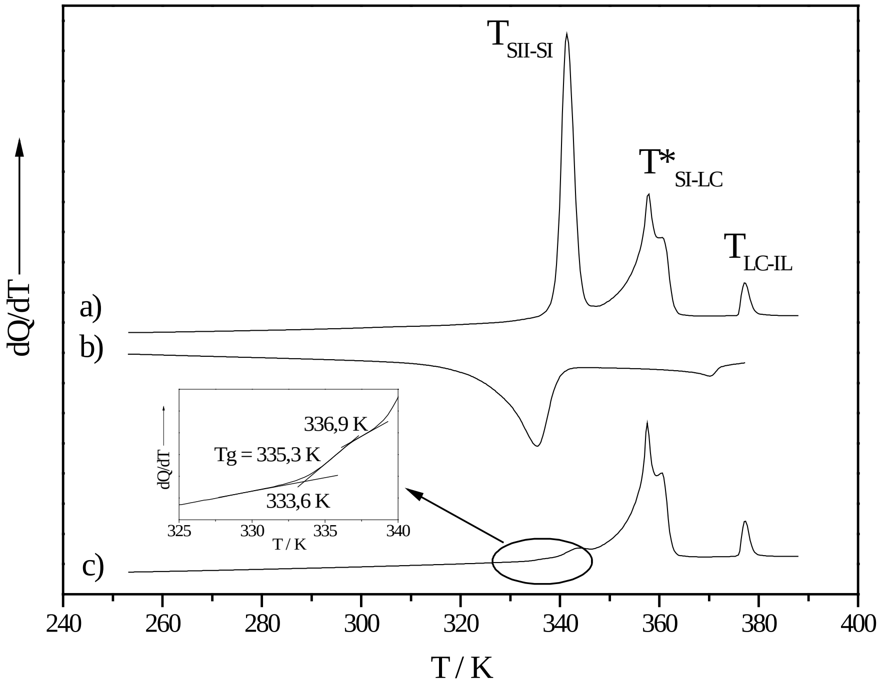

Figure S4. Thermograms of Pb(C7)$_2$ in the first heating (a), cooling (b) and second heating (c), all of them registered at 5 K·min^{-1}. The transition temperatures of SI-LC and LC-IL, and the Tg are indicated in the plot. * The transition SI-LC is fusion, that occurs in two steps (ref 1)

Table S1. Thermal data of the phase transitions for the short lead(II) alkanoates.

Pb(C*n*)$_2$	Transition	T / K	$\Delta_{trs}H$ / kJ·mol^{-1}	$\Delta_{trs}S$ /J·K^{-1}·mol^{-1}
Pb(C3)$_2$^{a}	*SII-IL*	398.2 ± 0.4	13.1 ± 0.1	32.9 ± 0.3
Pb(C4)$_2$^{a}	*SII-IL*	346.5 ± 0.3	14.7 ± 0.1	42.4 ± 0.3
	SI-IL*	322.8 ± 0.5	7.7 ± 0.4	32 ± 2
Pb(C5)$_2$^{b}	*SII-SI*	328.2 ± 0.6	8.8 ± 0.1	26.8 ± 0.4
	SI-IL	355.6 ± 0.3	12.6 ± 0.1	35.3 ± 0.3
Pb(C6)$_2$	*SII-LC*	339.3 ± 0.1	22.6 ± 0.1	66.6 ± 0.3
	LC-IL	354.2 ± 0.2	1.2 ± 0.1	3.4 ± 0.3
	SI-IL*	332.8 ± 0.4	(#)	
Pb(C7)$_2$	*SII-SI*	344.1 ± 0.1	16.5 ± 0.1	48.0 ± 0.3
	SI-LC (§)	355.9 ± 0.3	12.9 ± 0.1	36.2 ± 0.3
	LC-IL	372.9 ± 0.2	1.3± 0.1	3.5 ± 0.3

(§) fusion in two steps (ref 1); (#) Not measurable enthalpy (metastable transition).
[a] From reference 2, and [b] from reference 4.

2) X-ray Diffraction

Table S2. Experimental parameters and main crystallographic data for the compounds studied by single crystal XRD.

Data	Pb(C3)$_2$	Pb(C5)$_2$	Pb(C6)$_2$
Empirical Formula	$PbC_6H_{10}O_4$	$PbC_{10}H_{18}O_4$	$PbC_{12}H_{22}O_4$
Mr (g·mol^{-1})	353.33	409.43	437.49
Crystal system	monoclinic	triclinic	triclinic
Space group (No.)	$P2_1/m$ (11)	*P*-1 (2)	*P*-1 (2)
Crystal size (mm)	0.080 × 0.050 × 0.020	0.040 × 0.030 × 0.020	0.070 × 0.030 × 0.005
λ (Å)	0.9779	0.9779	0.7379
Temperature (K)	298(2)	100(2)	100(2)
a (Å)	4.771(1)	4.7440(9)	4.7400(9)
b (Å)	7.2100(14)	7.2110(14)	7.1920(14)
c (Å)	13.036(3)	17.982(4)	20.573(4)
α (°)	90	91.74(3)	86.98(3)
β (°)	97.76(3)	96.27(3)	84.79(3)
γ (°)	90	90.85(3)	89.18(3)
V (Å^3)	444.32(15)	611.1(2)	697.4(2)
Z	2	2	2
D_c (g·cm^{-3})	2.641	2.225	2.083
μ (mm^{-1})	18.95	13.80	12.096
Absorption correction	cylindrical	cylindrical	multi-scan
Reflection collected	361	888	2510
Reflections with $I > 2\sigma(I)$.	357	865	2495
Parameters refined /restrains	65 / 3	136 / 0	155 / 0
Hydrogen treatment	Not refined	Not refined	Not refined
R-factor	0.0715	0.0482	0.0499
wR2-factor	0.1713	0.1311	0.1428
Goodness of fit	1.085	1.088	1.038
CCDC deposition numbers	992161	992162	992163

Table S3. Experimental parameters and main crystallographic data for the compounds studied by powder XRD.

Crystal data	**Pb(C3)$_2$**	**Pb(C5)$_2$**	**Pb(C6)$_2$**
formula	$PbC_6H_{10}O_4$	$PbC_{10}H_{18}O_4$	$PbC_{12}H_{22}O_4$
Mr (g·mol^{-1})	353.33	409.43	437.49
cell setting, space group (no.)	monoclinic, $P2_1$/m (11)	triclinic, P-1 (2)	triclinic, P-1 (2)
temperature (K)	298(2)	298(2)	298(2)
a (Å)	4.77810(5)	4.82727(6)	4.83942(9)
b (Å)	7.21366(7)	7.27531(7)	7.30791(13)
c (Å)	13.05820(10)	18.08886(16)	20.6726(5)
α (°)	90	91.2653(13)	91.969(2)
β (°)	97.8573(9)	96.9135(10)	95.6808(17)
γ (°)	90	91.2613(13)	88.8359(17)
volume (Å^3)	445.859(7)	630.311(11)	726.98(3)
Z, D_c (g·cm^{-3})	2, 2.632	2, 2.157	2, 1.999
wavelength (Å)	1.54056	1.54056	0.8266(1)
μ (mm^{-1})	21.5	13.8	5.8
Data collection			
diffractometer	X'Pert PRO ALPHA1	X'Pert PRO ALPHA1	SpLine (BM25A, ESRF)
specimen mounting	borosilicate glass capillary		
data collection mode	transmission		
scan mode	2θ-step scan		
2θ range (°), step size (° 2θ)	2.5-85, 0.008	2.5-85, 0.008	1.0-40, 0.015
Refinement			
Refinement method	full-matrix least-squares on I_{net}		
profile function	pseudo-Voigt with axial divergence asymmetry		
R_p, R_{wp}, R_{exp}	0.1359, 0.1791, 0.1353	0.0957, 0.1243, 0.1072	0.0285, 0.0394, 0.0186
R_F, R_{BRAGG}	0.0454, 0.0633	0.0436, 0.0325	0.0481, 0.0424
goodness-of-fit	1.324	1.160	2.118
no. of contributing reflections	446	1126	997
no. of parameters	86	98	86
CCDC deposition number	992164	992165	992166

Table S4. Cell parameters for the short lead(II) alkanoates at 298 K.

Data	**Pb(C3)$_2$** [1]	**Pb(C4)$_2$** [2§]	**Pb(C5)$_2$** [2]	**Pb(C6)$_2$** [2]	**Pb(C7)$_2$** [1#]
Crystal system	monoclinic	monoclinic	triclinic	triclinic	triclinic
Space group (No.)	$P2_1/m$ (11)	$P2_1/m$ (11)	P-1 (2)	P-1 (2)	P-1 (2)
a (Å)	4.771(1)	4.80093(4)	4.82745(6)	4.83930(9)	4.8574(10)
b (Å)	7.2100(14)	7.26249(5)	7.27542(7)	7.30782(13)	7.3046(10)
c (Å)	13.036(3)	15.56795(16)	18.09025(15)	20.6733(5)	23.1846(10)
α (°)	90	90	91.2641(12)	91.971(2)	91.610(10)
β (°)	97.76(3)	96.9765(7)	96.9114(10)	95.6804(17)	95.660(10)
γ (°)	90	90	91.2639(13)	88.8349(17)	90.990(10)
V (Å^3)	444.32(15)	538.784(8)	630.395(11)	726.98(3)	818.1(2)

[1] Solved by SCXRD, and [2] solved by HRPD. § From reference 9; and # from reference 10.

Table S5. Pb-O and Pb- Pb distances for Pb(C3)$_2$ (at 298 K), and for Pb(C5)$_2$ and Pb(C6)$_2$ (both at 100 K), obtained from the SCXRD data.

Compound	Atom 1	Atom 2	Count	Distance / Å
Pb(C3)$_2$	Pb1	O2	1x	2.362(21)
		O1	1x	2.483(26)
		O3	2x	2.569(13)
		O3	2x	2.696(14)
		O1	1x	2.898(23)
	Pb1	Pb1	2x	4.3566(11)
		Pb1	2x	4.7710(17)
		Pb1	2x	4.9316(13)
Pb(C5)$_2$	Pb1	O2	1x	2.402(11)
		O1	1x	2.442(14)
		O3	1x	2.540(12)
		O4	1x	2.580(13)
		O3	1x	2.600(12)
		O4	1x	2.751(13)
		O1	1x	2.892(14)
	Pb1	Pb1	1x	4.3135(16)
		Pb1	1x	4.3361(15)
		Pb1	2x	4.7440(14)
		Pb1	1x	4.8048(17)
		Pb1	1x	4.8894(17)
Pb(C6)$_2$	Pb1	O1	1x	2.4132(62)
		O2	1x	2.4696(48)
		O3	1x	2.5280(43)
		O4	1x	2.5846(44)
		O3	1x	2.6039(47)
		O4	1x	2.7781(45)
		O2	1x	2.8604(46)
	Pb1	Pb1	1x	4.3002(13)
		Pb1	1x	4.3203(13)
		Pb1	2x	4.7400(9)
		Pb1	1x	4.7939(15)
		Pb1	1x	4.8769(14)

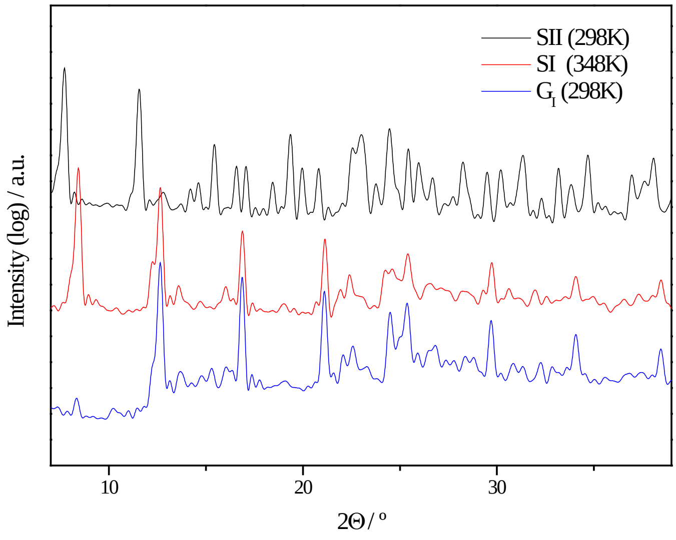

Figure S5. Diffraction patterns of Pb(C7)$_2$ in the crystal phase, SII (at room temperature), in the *rotator* phase, SI (at 348 K), and in the *rotator* glass state, G$_I$ (at room temperature, after cooling form the melt), showing the similarities between the structure of the two last ones. The intensity is in logarithmic scale for a better comparison of the diffractograms.

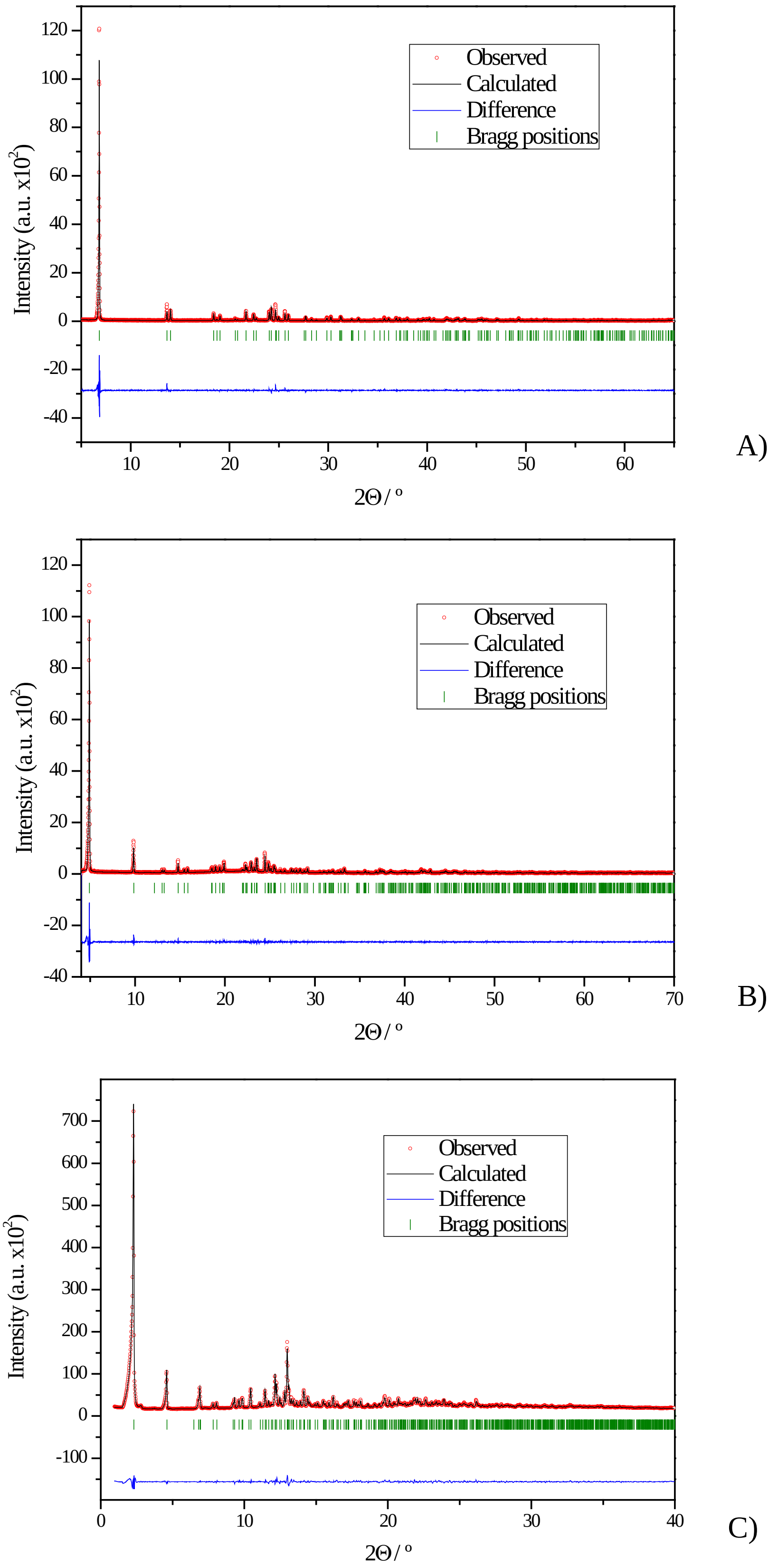

Figure S6. Rietveld refinement for Pb(C3)$_2$ (A), Pb(C5)$_2$ (B) and Pb(C6)$_2$ (C), showing the excellent agreement between the observed and calculated diffraction patterns, their difference, and Bragg positions.

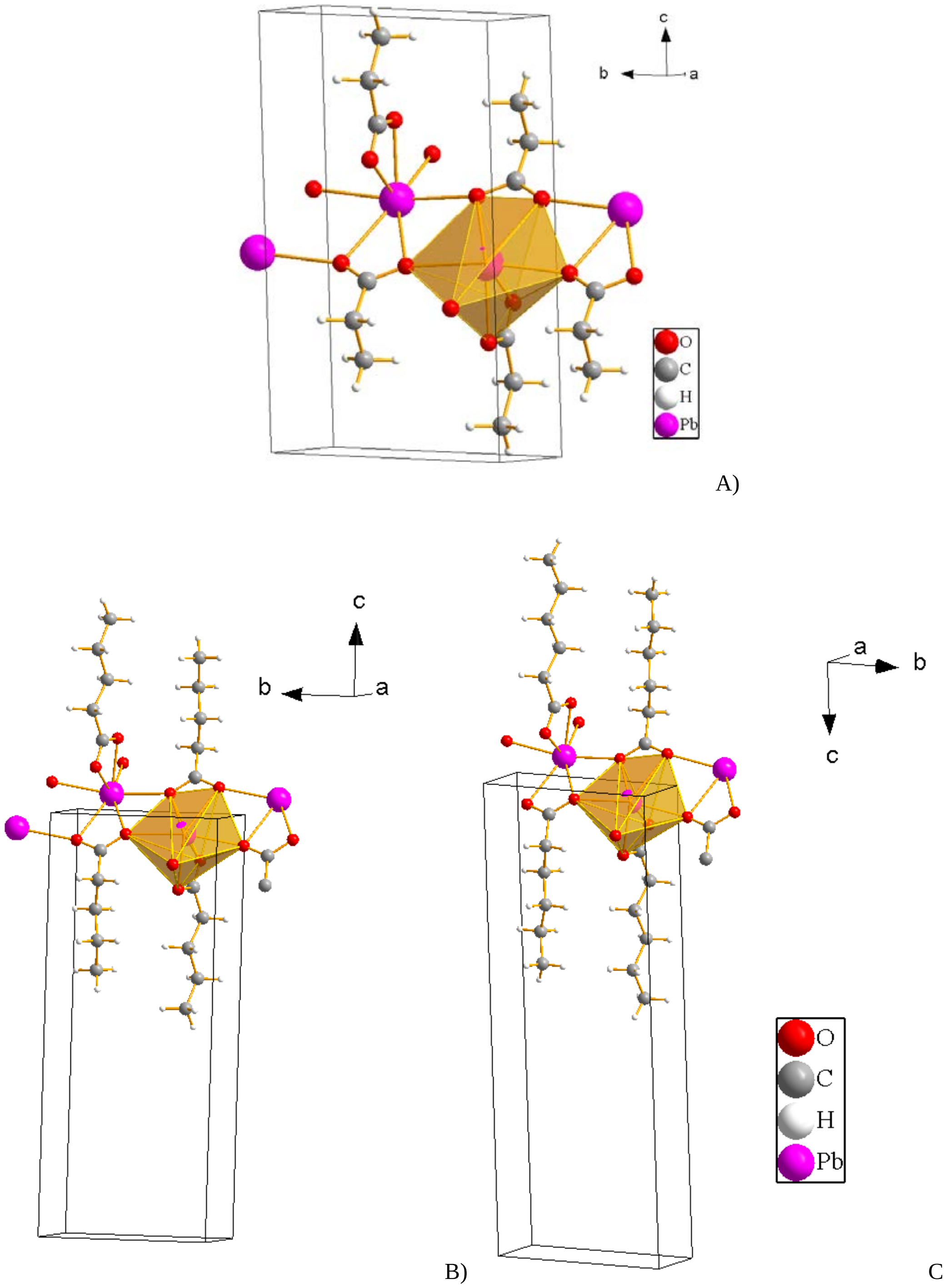

A)

B)

C)

Figure S7. Crystal structures obtained by SCXRD for Pb(C3)$_2$ (A), Pb(C5)$_2$ (B), and Pb(C6)$_2$ (C), showing the coordination polyhedron of the lead(II) atom (hemidirected geometry), in all of the cases, being seven the coordination number.

3) PDF Analysis

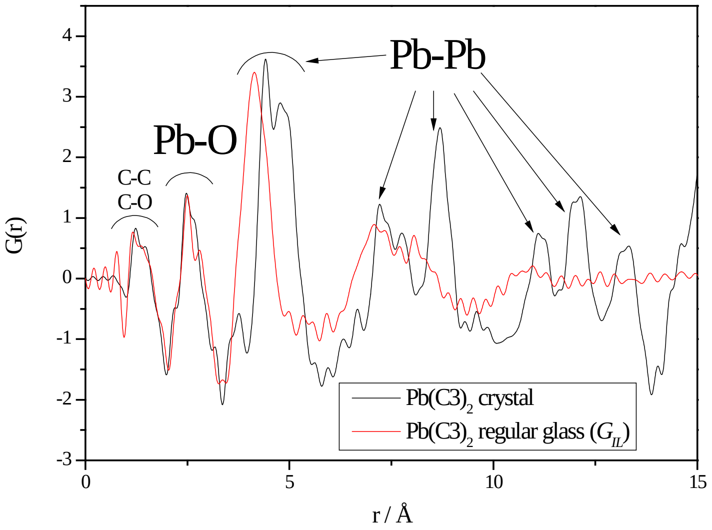

a)

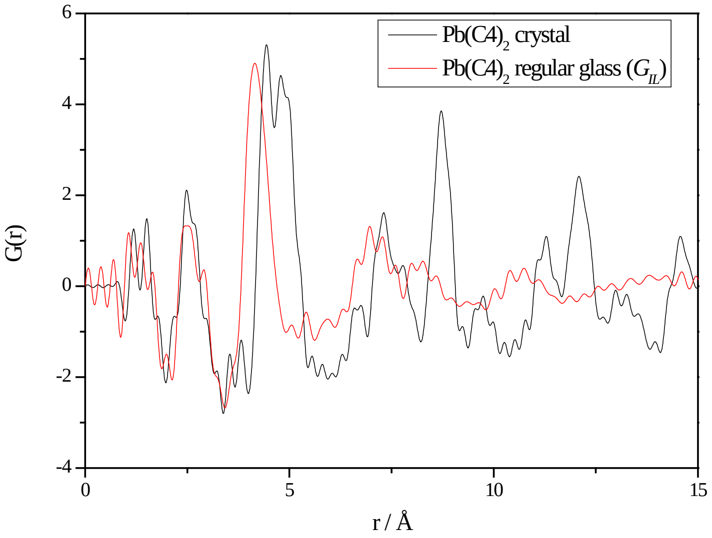

b)

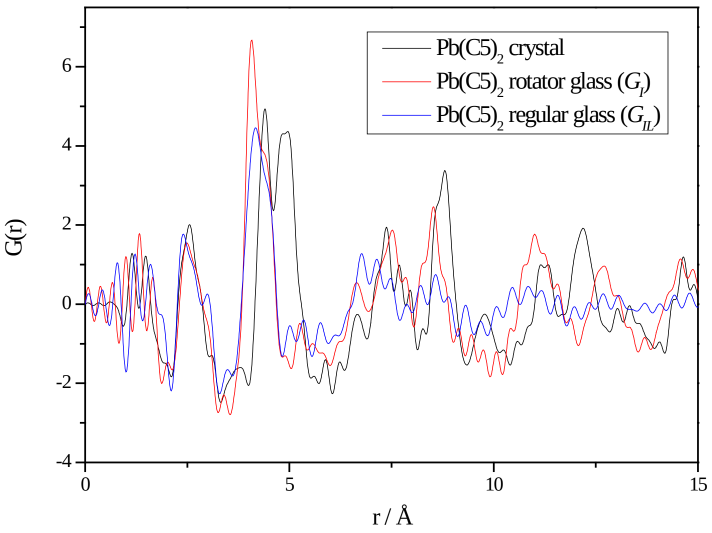

c)

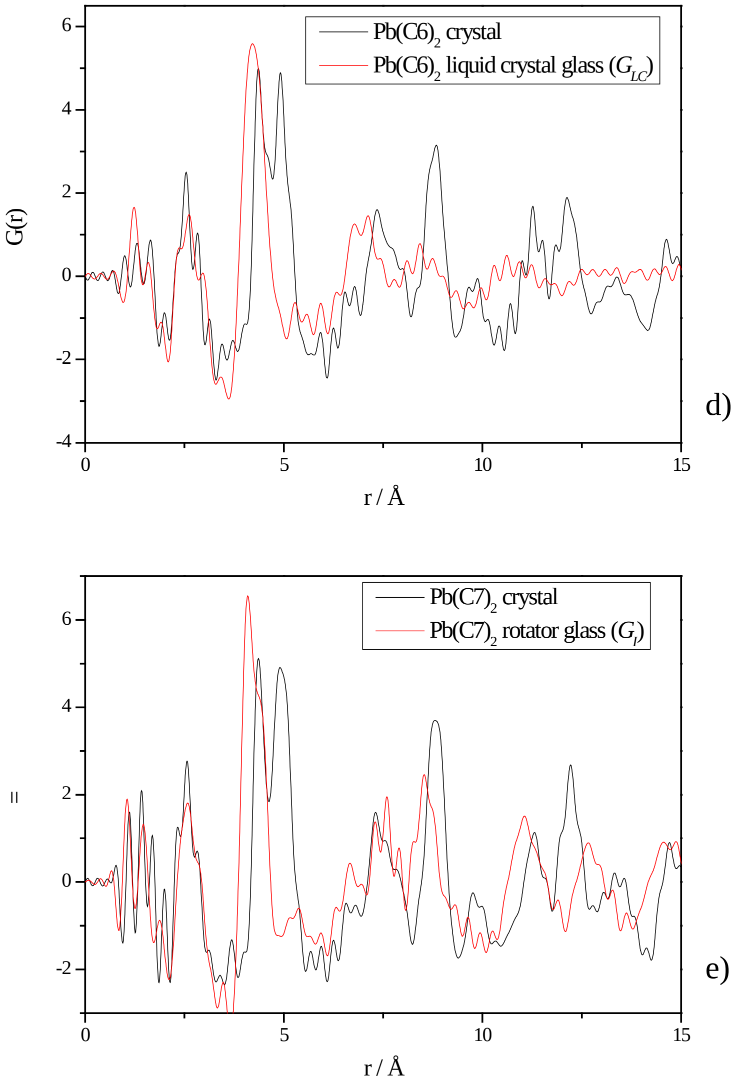

Figure S8. Pair Distribution Function (PDF) Analysis of high-energy X-ray total scattering data for the lead(II) alkanoates, from $Pb(C3)_2$ to $Pb(C7)_2$ (*a* to *e*) in the crystal and their corresponding glass phase(s), in the short distance range. The main distances between atoms, common for the 5 compounds, are shown in a).

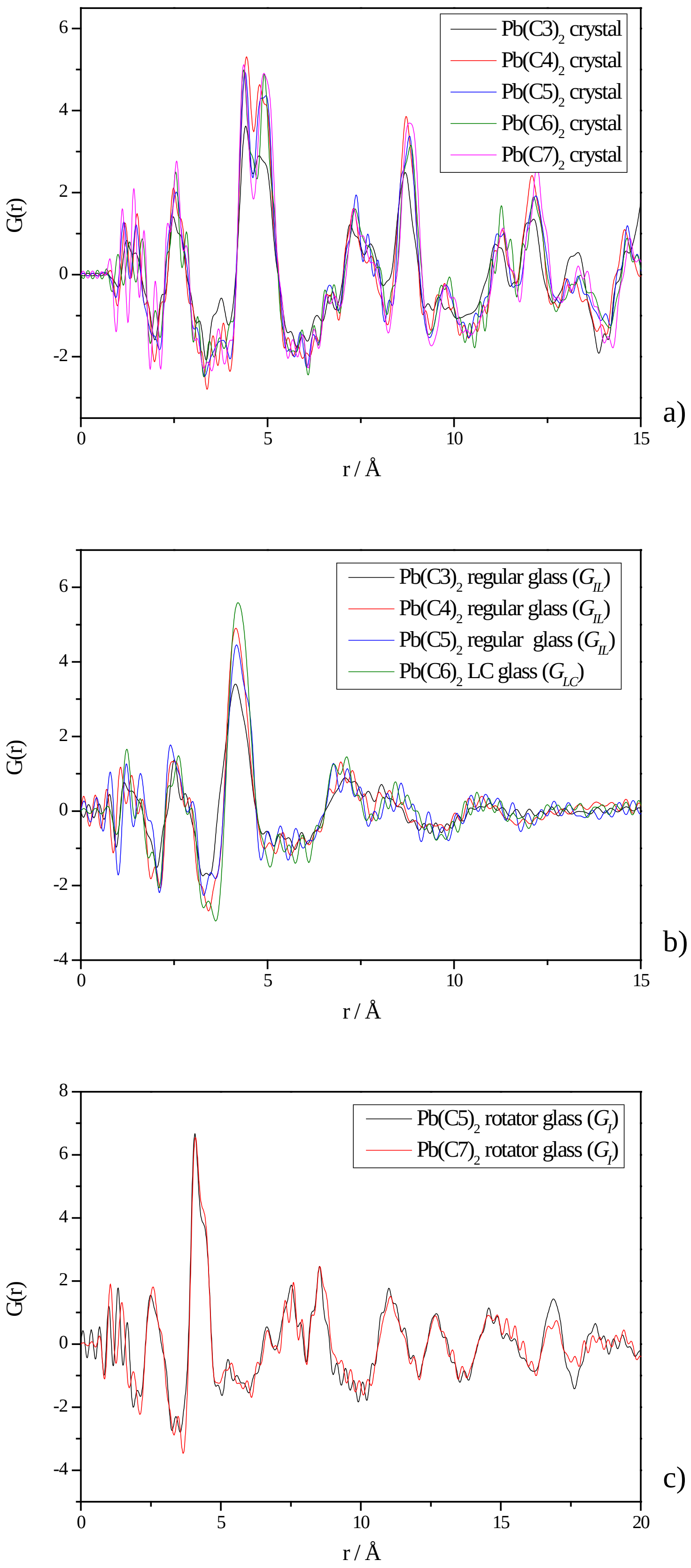

Figure S9. PDF Analysis, grouping by the different phases: crystal (a), regular and liquid crystal glass (b), and rotator glass (c).

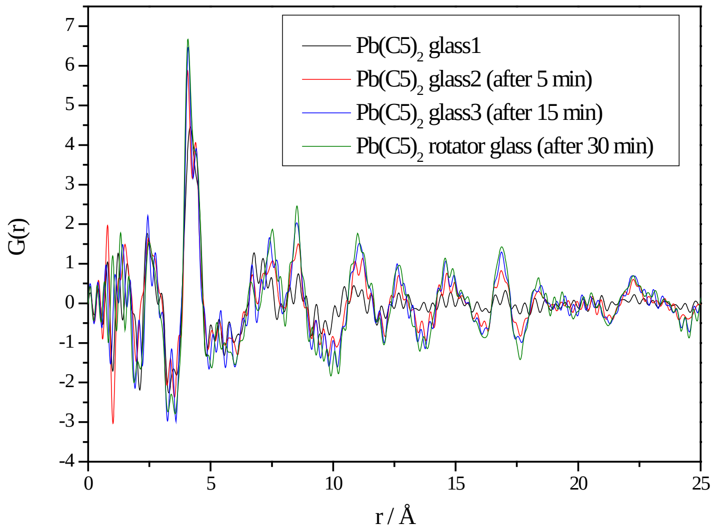

Figure S10. PDF Analysis of Pb(C5)$_2$, showing the evolution from the regular glass into rotator glass in a total time of 20 minutes (the lapse between each measurements is 5 minutes approximately).

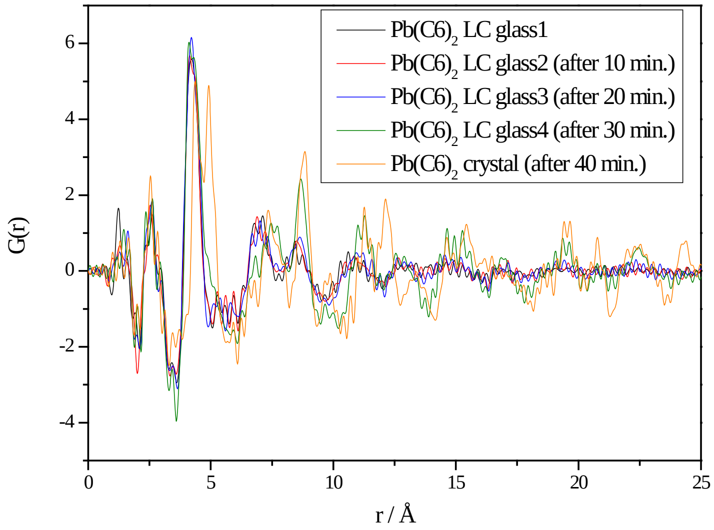

Figure S11. PDF Analysis of Pb(C6)$_2$, showing the partial conversion from the liquid crystal glass into the crystal phase. The lapse between each measurements is 10 minutes approximately, so in 40 minutes, a certain amount of LC glass is still present in the sample.

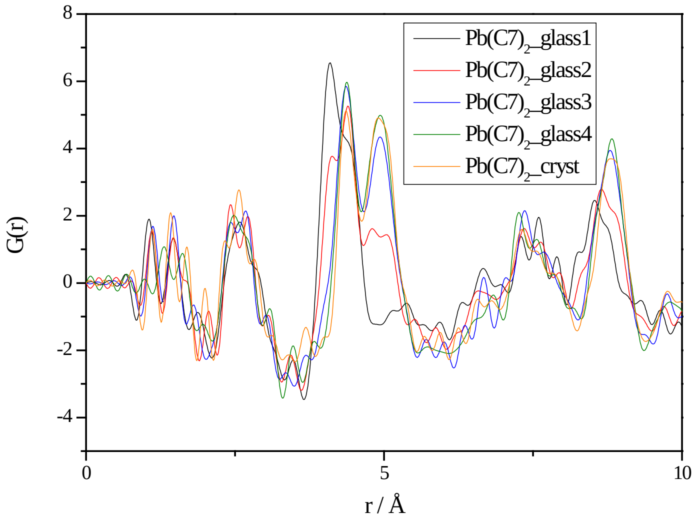

Figure S12. PDF Analysis of Pb(C7)$_2$, showing the evolution from the rotator glass into the crystal phase in a total time of 20 minutes (the lapse between each measurements is 5 minutes approximately).

4) Photoluminescence (PL)

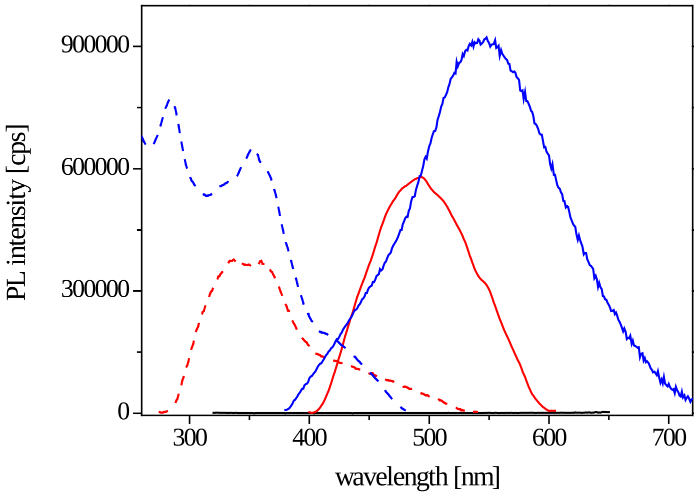

Figure S13. Photoluminescence excitation (dashed lines) and emission (solid lines) spectra of Pb(C3)$_2$, recorded in the crystal phase at 293 K (black) and 77 K (red) and in the glass phase (blue); for the emission spectra λ_{exc} = 300 nm, while for the excitation spectra λ_{em} = 560 nm.

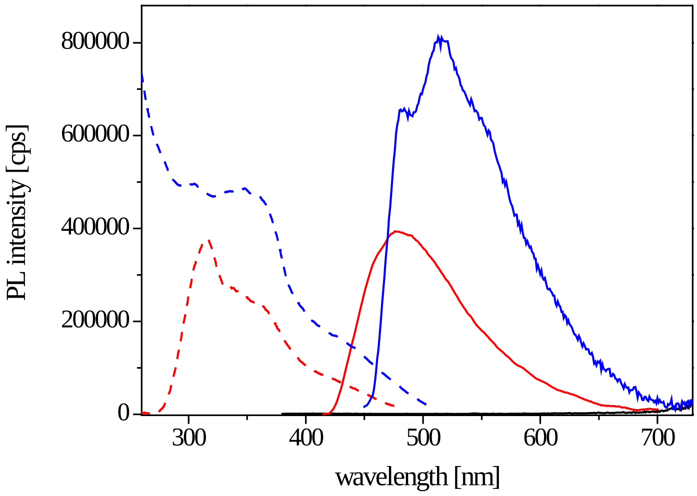

Figure S14. Photoluminescence excitation (dashed lines) and emission (solid lines) spectra of Pb(C5)$_2$, recorded in the crystal phase at 293 K (black) and 77 K (red) and in the glass phase (blue); for the emission spectra λ_{exc} = 300 nm, while for the excitation spectra λ_{em} = 520 nm.

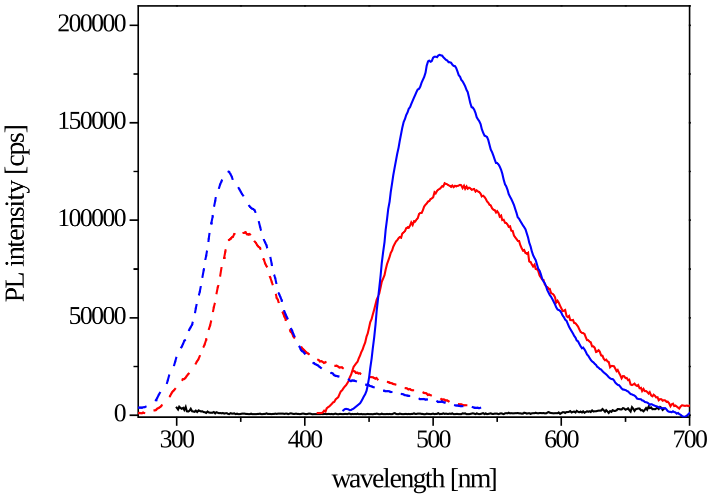

Figure S15. Photoluminescence excitation (dashed lines) and emission (solid lines) spectra of Pb(C6)$_2$, recorded in the crystal phase at 293 K (black) and 77 K (red) and in the glass phase (blue); for the emission spectra λ_{exc} = 350 nm, while for the excitation spectra λ_{em} = 550 nm.

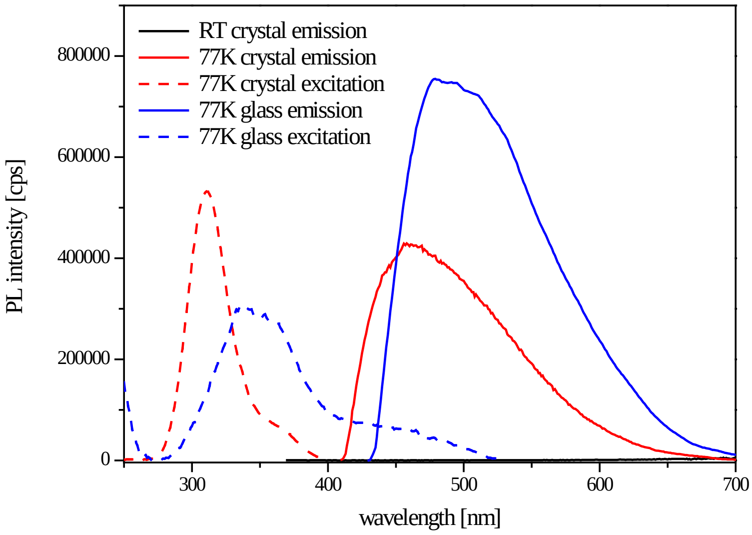

Figure S16. Photoluminescence excitation (dashed lines) and emission (solid lines) spectra of Pb(C7)$_2$, recorded in the crystal phase at 293 K (black) and 77 K (red) and in the glass phase (blue); for the emission spectra λ_{exc} = 350 nm, while for the excitation spectra λ_{em} = 550 nm.

5) C-13 CP/MAS NMR

Measurements of C-13 CP/MAS-NMR and powder XRD as a function of temperature were also carried out to check the similarities in the structures of the rotator phase (SI) and the rotator glass (G_I), where the only difference remains in the dynamic or static nature of the disorder, respectively.

Figure S17 illustrates the C-13 CP/MAS-NMR spectra of the crystal (SII) at 296 K, rotator (SI) at 344 K and rotator glass (G_I) at 298 K from 344 K phases of Pb(C7)$_2$. Seven groups of signals corresponding to the five carbon atoms in the compound, from the carboxylate centered at ~184 ppm to the methyl group centered at ~15 ppm, are observed.

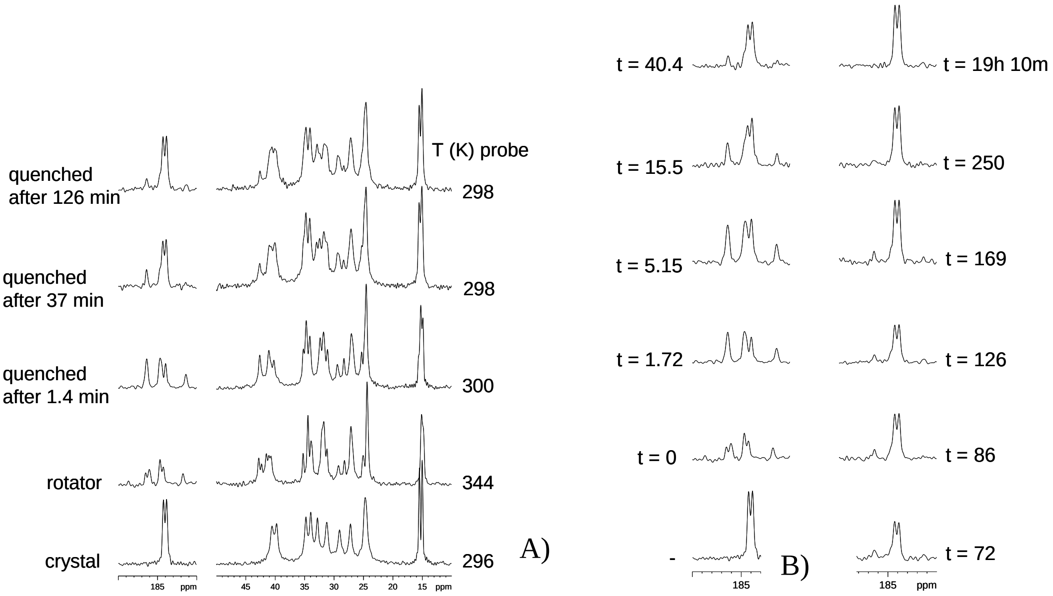

Figure S17. C-13 CP/MAS-NMR spectra of Pb(C7)$_2$: A) showing the crystal (SII) at RT, the rotator phase (SI) at 344 K, and the rotator glass (GI), quenched and after the indicated time; B) signal corresponding to the carboxylate group showing the formation of the crystal phase (SII) from the rotator glass (GI) after the time indicated (in minutes).

In the spectrum taken on the crystal (SII), all of the bands appear as doublets with the approximate same area, whereas in the one corresponding to the rotator phase (SI), the doublets associated to the carbons at the end of the chain (methyl and methylene) collapse into a singlet and multiplicity increases for the rest of the carbons. Subsequently the sample was quenched in a CO_2 ice/isopropanol mixture, placed again in the magnet, and measured again at 296 K. This thermal treatment freezes the disorder introduced by the thermal changes and leads to a very similar spectrum to the one at 344 K. The same result was seen by XRD as a function of temperature, and very similar diffraction patterns are obtained in the rotator phase and in the rotator glass (immediately measured at room temperature after melting the sample, Fig. S5).

However, the rotator glass, G_I, converts into the crystal phase (SII) in a short time. Thus, NMR spectra were recorded in the glass state at room temperature at different times, and a quick conversion into SII was observed (Fig. S17B): from 250 minutes on, the signal, corresponding already to the SII phase, remains constant. On the other hand, G_I is much more stable in time at room temperature in the case of Pb(C5)$_2$.[4Error! Bookmark not defined.] In the PDF analysis for Pb(C7)$_2$, the conversion from the rotator glass to the crystal phase was observed in aprox. 20 min.

6) Polarized Light Microscopy

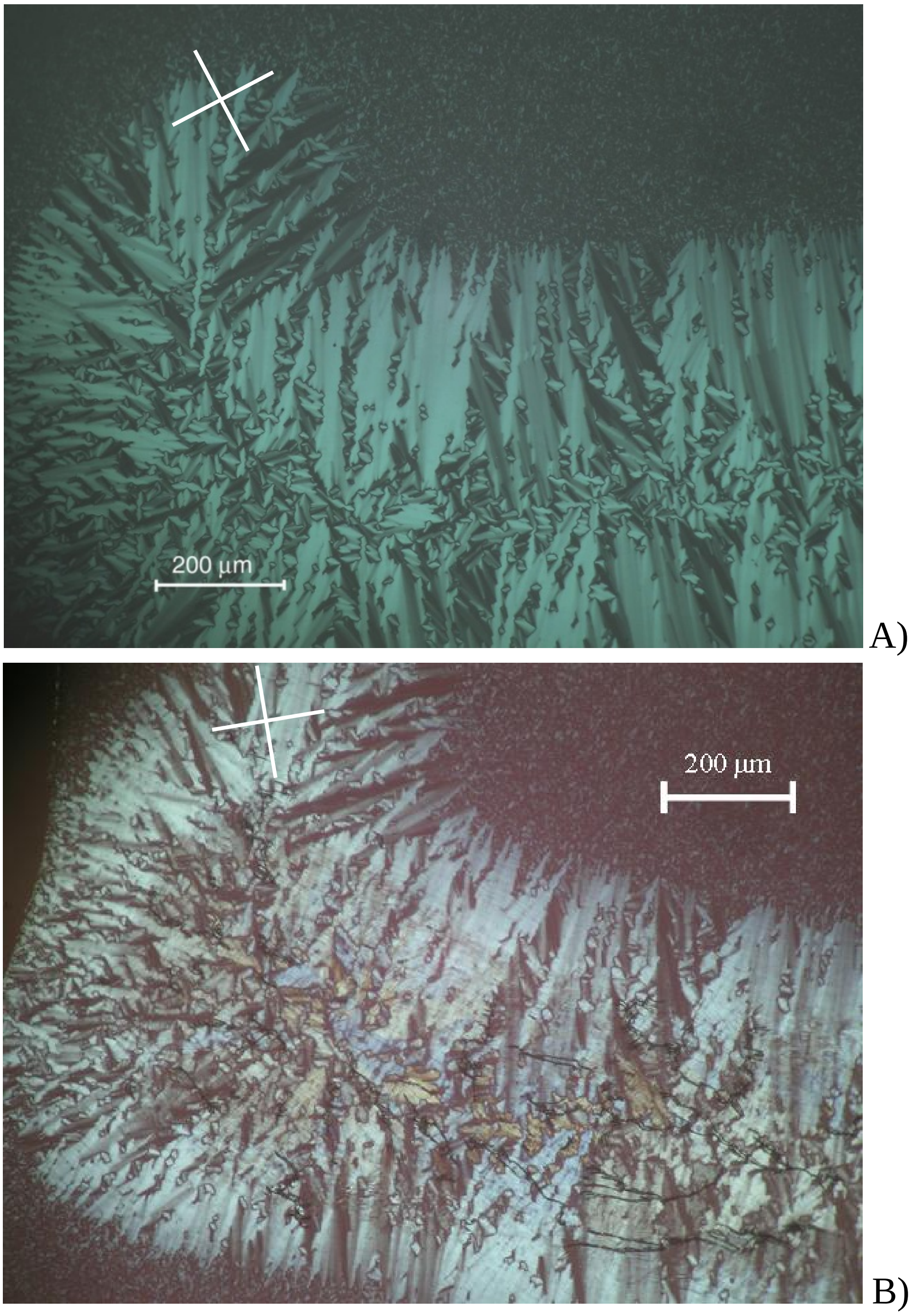

Figure S18. Pictures of Pb(C6)$_2$ A) in the liquid crystals phase (LC), at 350 K, showing the typical fan shape domains of a “smectic A like” (or neat phase); and B) in the undercooled liquid crystal phase (LC’), at room temperature (after cooling the sample below the Tg), where a partial conversion to a solid phase may be present in the middle of the picture. White crosses show the orientation of the crossed polars.

■ REFERENCES

1 Sánchez Arenas, A; García, M. V.; Redondo, M. I.; Cheda, J. A. R.; Roux, M. V.; Turrión, C. *Liq. Cryst.* **1995,** *18*, 431-441.

2 Martínez-Casado, F. J.; Sánchez Arenas, A.; García Pérez, M. V.; Redondo Yélamos, M. I.; López de Andrés, S.; Cheda, J. A. R. *J. Chem. Therm.* **2007**, *39*(*3*), 455-461.

3 Martínez Casado, F. J.; Ramos Riesco M.; Da Silva, I.; Redondo, M. I.; Labrador, A.; Cheda, J. A. R. *Cryst. Growth Des.* 2011, **11**(3), 759–767.

4 Martínez Casado, F. J.; Ramos Riesco M.;Sánchez Arenas, A.; García Pérez, M. V.; Redondo, M. I.; López-Andrés, S.; Garrido, L.; Cheda, J. A. R. *J. Phys. Chem. B* 2008, **112**(51), 16601–16609.

5 Sheldrick, G.M. Acta Crystallogr., Sect. A 2008, 64, 112-122.

6 Chupas, P. J.; Qiu, X. Y.; Hanson, J. C.; Lee, P. L.; Grey, C. P.; Billinge, S. J. L. J. Appl. Crystallogr., 2003, 36, 1342–1347.

7 a) Hammersley, A. P.; Svensson, S. O.; Hanfland, M.; Fitch, A. N.; Hausermann D. High Press. Res., 1996, 14 (4–6), 235–248; b) Fit2D V9.129 Reference Manual V. 3.1; Hammersley A. P. In ESRF Internal Report, ESRF98HA01T, 1998.

8 Juhás P.; Davis, T.; Farrow, C. L.; Billinge S. J. L. J. Appl. Cryst., 2013, 46, 560-566.

9 Martínez Casado, F. J.; Ramos Riesco M.; Da Silva, I.; Redondo, M. I.; Labrador, A.; Cheda, J. A. R. *Cryst. Growth Des.* 2011, **11**(3), 759–767.

[10] Lacouture, F.; Francois, M.; Didierjean, C.; Rivera, J. P.; Rocca, E.; Steinmetza, J. *Acta Cryst*. **2001** *C57*, 530-531.